JOURNAL OF CRITICAL REVIEWS

ISSN- 2394-5125 VOL 7, ISSUE 15, 2020

Evaluation of histogram based thresholding methods with morphological operations for lung segmentation

R. Jenkin Suji[1*], Sarita Singh Bhadauria[2]

[1]ABV-IIITM Gwalior,

[2]RGPV Bhopal,

[1]sujijenkin@gmail.com

[2]saritasmits61@yahoo.co.in

Received: 12 May 2020 Revised and Accepted: 07 July 2020

Abstract: To develop a process for lung segmentation from CT volume images, six different thresholding algorithms were evaluated and compared for their ability to separate the lung parenchyma from the non-lung region. This work briefly discusses the six techniques used for the same. These six well known thresholding algorithms were applied on image sets from the Kaggle "Finding and Measuring Lungs in CT Data" dataset and compared, to find the most effective method. The validation of the thresholding algorithms was performed by dividing the image volume into four quadrants. It is inferred that fixed thresholding approach outperforms other approaches consistently and the main reason for failure of other automatic thresholding approaches is due to the varying distribution of the lung and non-lung pixel intensities over the lung volume.

Keywords: Thresholding, CT Scan, Lung Segmentation, Lung Cancer, ROC, Recall-Precision Curve

I. Introduction

In India, Lung cancer accounts for second largest number of cancer related deaths in men and fourth largest in women [1]. One of the main reasons cited for high mortality in lung cancer is late diagnosis. Early diagnosis of lung cancer reduces the number of related deaths and increases the survival rate. Further, early detection of lung cancer plays a challenging as well as a significant role in lung cancer diagnosis and prognosis. Medical Imaging techniques use non invasive procedures through different imaging modalities like Computed Tomography (CT), Low Dose Computed Tomography (LDCT), Magnetic Resonance Imaging (MRI), Positron Emission Tomography (PET) etc [2]. Pulmonary nodules are one of the major symptoms of lung cancer which may be picked from CT Images [3]. Thin Slice CT Images are very useful in identifying the nodules at increased speed, resolution and better accuracy [4]. Computer based systems for lung nodule detection and diagnosis also augment the radiologists and physicians by offering a faster way of detecting the nodules and identify the better treatment plans to improve the survival rate.

Lung segmentation is one of the preliminary steps in a computer based system for lung cancer detection and diagnosis (CAD), also called Computer Aided Diagnosis system. Proper Lung segmentation narrows the search space for nodule detection thereby reducing the computation resources required. While lung segmentation is advantageous, it also poses it share of challenges due to the nature of the images from various image capturing devices, imaging protocols, modalities as well as the structure of the lung, position of the nodules etc.

Segmentation algorithms are broadly classified into thresholding based, region based, model based and machine learning based methods. Thresholding methods are simple and widely used in segmenting the lung structures. The major drawback of thresholding methods are over and under segmentation. Despite their inconveniences, thresholding methods are widely used in lung segmentation in conjuction with other image processing operations. Hence, an analysis of the thresholding methods within the context of lung segmentation is necessary to build an efficient computer based system for lung cancer detection and diagnosis.

The major contributions of this paper are the following:

1. This work presents a comparative evaluation of various thresholding methods in a thresholding and morphological operation based pipeline for lung segmentation.

ISSN- 2394-5125 VOL 7, ISSUE 15, 2020

2. This work quantitatively analyses the results on using variants of thresholding approaches for lung segmentation.

3. This work generates the ROC and Recall-Precision curve by applying various thresholds on a single volume and analyses the same.

The performance of these thresholding methods were evaluated based on sensitivity, specificity, accuracy, precision, recall, receiver operating characteristics and area under the curve. This paper presents the analysis of various thresholding methods. Section II describes the literature survey of thresholding methods for lung segmentation, Section III describes various thresholding based methodology of lung segmentation based on various lung segmentation methods followed by results and discussions discussed in section IV. Finally section V concludes with conclusion and future directions.

II. Literature Survey

Medical image segmentation extracts or segments the foreground (i.e) region of interest from the background using semi-automatic or automatic segmentation methods. Thresholding methods use a fixed/adaptive threshold for segmenting the lung structures. Proper selection of threshold is very essential for good segmentation results. Multi-thresholding uses more than one threshold values for segmenting the multiple objects as a interest [5]. The drawback of the thresholding methods does not consider the spatial information and it leads to sensitivity to noise and inhomogenities. Thresholding methods can be classified into global thresholding and local thresholding. Global thresholding selects a threshold considering that image has a bimodal histogram. Local thresholding methods are adaptive thresholding methods which uses a local threshold or Otsu threshold for segmenting the lung structures. Global thresholding fails to segment the images properly when the images do not have a constant background and local thresholding overcomes this problem by selecting a local threshold. On the other hand, local thresholding requires more computation time.

Some of the traditional methods in the literature for lung segmentation are optimal thresholding [6], region growing algorithm [7], morphological filters [7], connected component analysis (CCA) [8], fuzzy c-means (FCM) clustering and local energy constraint (LEC) [9], OTSU thresholding method [10], edge detection [11], and rolling ball algorithm [12] and deformable models mainly refer to active contour models [13].

Senthilkumaran and Vaithegi [14] compared two local thresholding methods such a niblack and sauvola and evaluated its performance measures in terms of jaccard similarity coefficient and peak signal to noise ratio [14]. Sahoo et al [15] tested the performance of various global thresholding based on uniformity and shape measures on real images. Mansoor et al [16] reviewed the various lung segmentation methods from low to high pathological conditions of the lung.

As such, there are not much literature that exist, quantitatively verifying various lung segmentation approaches. This work bridges the gap.

III. Methodology

Lung segmentation involves segmenting the lung which means to delineate (or) separate the lung from the surrounding organs and structures such as the heart, rib cage, and diaphragm. The segmented lung comprises of parenchyma, which is a cellular tissue lying between the lung body wall and the organs. This is present in two lobes – right lobe and left lobe.

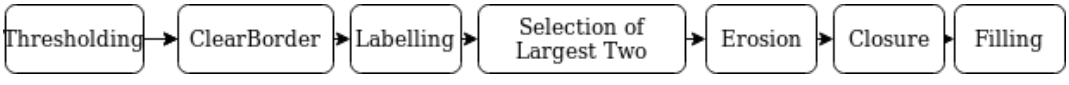

Figure 1. Pipeline for lung segmentation

Lung Parenchyma segmentation is one of the important step for further detecting the lung nodules accurately. The pipeline used in this entire work for lung segmentation is given in figure 1 and is closely based on [17]. This work primarily focuses on the first step, thresholding. Thresholding divides the input image into foreground and background by converting a single channel 2-D image made of Hounsfield pixel intensities into a binary image.

ISSN- 2394-5125 VOL 7, ISSUE 15, 2020

The second step is clear border where the blobs connected to the border of the image are removed. The third step in the pipeline is labelling when all the connected regions of the binary image are labelled. In the fourth step the area of all the connected regions are computed and the two largest regions of the binary image are selected to become foreground and rest of the connected regions become the background.

As the fifth step, the resultant image is applied with erosion operation, which separates the separates the lung nodules attached to the blood vessels. This operation uses a 2-d disk of size 2. As the sixth step, closure operation is applied so that the lung nodules are kept attached to the lung nodule.

As the seventh step, filling operation is performed, to fill small holes in the binary lung mask and the resultant image is the segmented lung mask.

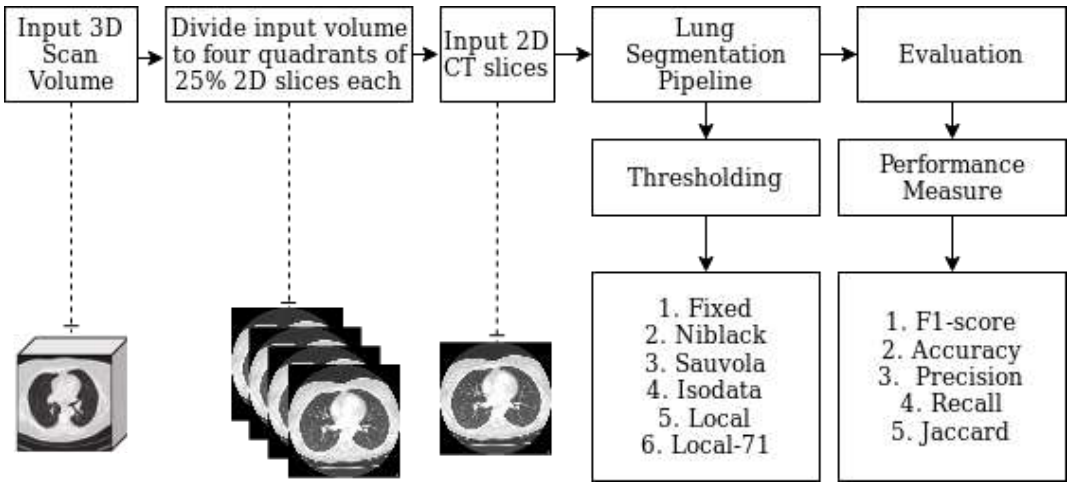

Figure 2. Overall Methodology with different types of thresholding and performance measure

Figure 2 depicts the overall process carried out in this work. The 3D input CT volume is split into multiple 2D slices and each 2D slice is given as input to the segmentation block for segmenting the lung parenchyma from the background. This work applies following six automatic thresholding approaches and evaluates the result using the depicted five evaluation measures.

The different thresholding variants are used in this paper for comparision and are explained below.

1. Fixed Thresholding – The HU of air is -1000, water is 0 and the lung structures varies between -700 to -500. A fixed value of -400 HU is selected as threshold.

2. Niblack Thresholding [19] – Niblack local image thresholding uses an integral image method, which guarantees constant computation time regardless of the neighborhood size.

3. Sauvola Thresholding [20] - Sauvola method is a variation of Niblack, uses integral images for fast computation of the threshold function.

4. Isodata Thresholding [21] – Isodata method considers a threshold t, computes the average of, gray values with mean of all pixels less then or equal to t and the mean of all pixels with gray value greater than t.

5. Local Thresholding [22] – This method establishes the threshold at a regional level. The region sampled and method of evaluation vary between applications. This uses region block-size of 35. Adaptive thresholding at a pixel level (in comparison with neighboring pixels) can yield highly superior results compared to global thresholding, particularly for images with varying levels of regional contrast differences.

6. Local-71 Thresholding [22] – This is also a local thresholding which uses region block-size of 71.

ISSN- 2394-5125 VOL 7, ISSUE 15, 2020

The evaluation measures used in this work for evaluating the lung segmentation variants are the following:

1. F1 Score: harmonic mean of precision and recall [2(PxR)/(P+R)] where P and R stand for Precision and Recall.

2. Precision: How many pixels/voxels detected are actually part of the lung region? [TP/(TP + FP)]

3. Recall/Sensitivity/True Positive Rate: What fraction of the total lung pixels/voxels were detected? [TP/(TP+FN)]

4. Accuracy : How accurate is the algorithm detecting the lung region. [(TP+TN)/(TP+TN+FP+FN)]

5. Specificity : How accurate does the algorithm detect as negative if the region is non-lung region. [TN/(TN+FP)], where TN, TP, FN, FP are the respective counts of the decisions True Negative, True Positive, False Positive and False Negative.

6. ROC : Receiver Operating Characteristic: ROC curve characterizes the performance of the human observer for the given diagnostic task. The curve is plotted between False Positive Rate (FPR) in the x-axis and True Positive Rate (TPR) in the y-axis. False Positive Rate can be defined as the fraction of lung region diagnosed as non-lung region. True Positive Rate is the fraction of lung region cases diagnosed as lung region. ROC curve predicts the operating characteristics by moving the operating point and radiologist readings.

7. Recall-Precision Curve : The precision-recall curve shows the tradeoff between precision and recall for different threshold. A high area under the curve represents both high recall and high precision, where high precision relates to a low false positive rate, and high recall relates to a low false negative rate.

IV. Results and Discussion

The experiments were performed on "Finding and Measuring Lungs in CT Data" dataset [18] which is a collection of CT thoracic images whose lungs have been manually segmented lungs and measurements are both in 2D and 3D. There are only four 3D scans with 117,301,325 and 465 slices respectively. Each slice has a dimension of 512 x 512 voxels and intensity values are in Hounsfield units. Ground truth images with corresponding dimensions are also given. This work focuses applies the lung segmentation pipeline with some thresholding approaches only on the 3D scans. 3D scan volumes comprising multiple 2D scans were chosen as the images for evaluation since they offer scans of widely varying intensity distributions and histogram based approaches are normally affected by such variations. Instead of global thresholding, the thresholding was applied on individual slices and the results are shown in tables 1 to 4.

The tables 1 to 4, running over two rows each are divided into four large columns each with title Image 0, Image 1, Image 2 and Image 3. Each large column of the table corresponds to four scan volumes. Each of the four tables correspond to the results obtained by applying the thresholding techniques on 25% of each of the volumes. First table corresponds to first 25% across all four image volumes, second table corresponds to second 25 % and so on. Each large column is divided into five smaller columns corresponding to five evaluation metrics such as F1-score, Accuracy score, Precision score, Recall score and Jaccard score.

It can be observed from tables 1 to 4 that barring minor variations and few consistencies, the performance of every thresholding approach is consistent across all evaluation metrics over multiple portions of the image volume. For instance, across the image volume 0, Fixed, Isodata and Local-71 thresholding methods perform comparably well across all four tables. This is evident by observing under the column, Image 0 along the four tables. Similarly other image columns may also be observed. Savola and Niblack are the most poorly performing approaches among all the compared approaches, due to their poor metrics across all images.

Table 1.Quantitative results (F1, Accuracy, Precision, Recall and Jaccard Scores) on first quadrant images of 4 different scan volumes

ISSN- 2394-5125 VOL 7, ISSUE 15, 2020

S.No	Method	Image 0 (325 slices; First 25% - 82 slices)					Image 1 (465 slices; First 25% - 117 slices				
		FS	AS	PS	RS	JS	FS	AS	PS	RS	JS
1	Fixed	0.62	1	0.71	0.56	0.56	0.37	1	0.43	0.33	0.32
2	Sauvola	0.04	0.63	0.04	0.12	0.03	0.02	0.67	0.01	0.26	0.01
3	Ni Black	0.35	0.94	0.61	0.32	0.25	0.16	0.97	0.19	0.24	0.1
4	Isodata	0.65	1	0.72	0.61	0.58	0	0.98	0	0	0
5	Local	0.54	0.97	0.54	0.64	0.45	0.22	0.96	0.2	0.4	0.15
6	Local-71	0.57	0.98	0.53	0.68	0.51	0.3	0.97	0.29	0.47	0.24

S.No	Method	Image 2 (301 slices, First 25% - 76 slices)					Image 3 (117 slices, First 25% - 30 slices)				
		FS	AS	PS	RS	JS	FS	AS	PS	RS	JS
1	Fixed	0.15	0.99	0.15	0.14	0.13	0.23	1	0.26	0.23	0.19
2	Sauvola	0.01	0.65	0.01	0.01	0.01	0.02	0.71	0.01	0.27	0.01
3	Ni Black	0.1	0.99	0.14	0.1	0.07	0.07	0.99	0.08	0.1	0.04
4	Isodata	0.15	0.99	0.15	0.14	0.13	0	1	0	0	0
5	Local	0.12	0.99	0.11	0.14	0.1	0.11	0.97	0.08	0.29	0.07
6	Local-71	0.12	0.98	0.1	0.2	0.09	0.09	0.94	0.06	0.33	0.05

Table 2.Quantitative results (F1, Accuracy, Precision, Recall and Jaccard Scores) on second quadrant images of 4 different scan volumes

S.No	Method	Image 0 (325 slices; Second 25% - 81 slices)					Image 1 (465 slices; Second 25% - 116 slices				
		FS	AS	PS	RS	JS	FS	AS	PS	RS	JS
1	Fixed	0.98	0.99	1	0.95	0.95	0.97	0.99	1	0.95	0.95
2	Sauvola	0.12	0.66	0.1	0.15	0.08	0.1	0.67	0.08	0.14	0.06
3	Ni Black	0.38	0.83	0.92	0.25	0.24	0.24	0.85	0.68	0.15	0.14
4	Isodata	0.98	0.99	1	0.96	0.96	0	0.83	0	0	0
5	Local	0.93	0.97	0.93	0.93	0.88	0.7	0.93	0.78	0.68	0.6
6	Local-71	0.97	0.99	0.97	0.98	0.94	0.94	0.98	0.97	0.92	0.89

S.No	Method	Image 2 (301 slices, Second 25% - 75 slices)					Image 3 (117 slices, Second 25% - 29 slices)				
		FS	AS	PS	RS	JS	FS	AS	PS	RS	JS
1	Fixed	0.97	0.99	1	0.94	0.94	0.94	0.99	1	0.9	0.89
2	Sauvola	0.01	0.59	0.01	0.01	0.01	0.01	0.7	0.01	0.02	0.01
3	Ni Black	0.3	0.83	0.98	0.18	0.18	0.3	0.89	0.89	0.19	0.18
4	Isodata	0.97	0.99	1	0.95	0.94	0	0.87	0	0	0
5	Local	0.73	0.94	0.95	0.65	0.64	0.8	0.96	0.85	0.78	0.68
6	Local-71	0.9	0.98	0.94	0.87	0.84	0.81	0.96	0.79	0.86	0.7

Table 3.Quantitative results (F1, Accuracy, Precision, Recall and Jaccard Scores) on third quadrant images of 4 different scan volumes

S.No	Method	Image 0 (325 slices; Third 25% - 81 slices)					Image 1 (465 slices; Third 25% - 116 slices				
		FS	AS	PS	RS	JS	FS	AS	PS	RS	JS
1	Fixed	0.98	0.99	1	0.96	0.95	0.98	1	1	0.96	0.95
2	Sauvola	0.01	0.79	0.01	0.01	0.01	0.18	0.75	0.14	0.26	0.14
3	Ni Black	0.28	0.84	0.93	0.17	0.17	0.31	0.86	0.92	0.19	0.19
4	Isodata	0.98	1	1	0.96	0.96	0	0.83	0	0	0
5	Local	0.82	0.95	0.9	0.79	0.74	0.85	0.96	0.92	0.81	0.78
6	Local-71	0.97	0.99	0.96	0.98	0.93	0.84	0.96	0.89	0.81	0.77

S.No	Method	Image 2 (301 slices, Third 25% - 75 slices)					Image 3 (117 slices, Third 25% - 29 slices)				
		FS	AS	PS	RS	JS	FS	AS	PS	RS	JS
1	Fixed	0.98	0.99	1	0.96	0.96	0.97	0.99	1	0.94	0.93
2	Sauvola	0.01	0.63	0.01	0.01	0.01	0.01	0.69	0.01	0.01	0.01
3	Ni Black	0.31	0.76	1	0.19	0.19	0.26	0.84	0.9	0.16	0.16
4	Isodata	0.98	0.99	1	0.96	0.96	0	0.82	0	0	0
5	Local	0.88	0.95	0.99	0.83	0.82	0.79	0.94	0.91	0.73	0.69
6	Local-71	0.97	0.99	1	0.95	0.94	0.95	0.98	0.94	0.95	0.89

Table 4.Quantitative results (F1, Accuracy, Precision, Recall and Jaccard Scores) on fourth quadrant images of 4 different scan volumes

ISSN- 2394-5125 VOL 7, ISSUE 15, 2020

S.No	Method	Image 0 (325 slices; Last 25% - 81 slices)					Image 1 (465 slices; Last 25% - 116 slices				
		FS	AS	PS	RS	JS	FS	AS	PS	RS	JS
1	Fixed	0.63	1	0.66	0.61	0.6	0.8	1	0.83	0.77	0.76
2	Sauvola	0	0.96	0	0	0	0	0.92	0	0	0
3	Ni Black	0.16	0.96	0.48	0.14	0.1	0.12	0.93	0.42	0.09	0.07
4	Isodata	0.64	1	0.66	0.63	0.61	0	0.93	0	0	0
5	Local	0.22	0.96	0.29	0.23	0.16	0.36	0.95	0.37	0.37	0.31
6	Local-71	0.38	0.97	0.35	0.46	0.32	0.29	0.92	0.3	0.34	0.21

S.No	Method	Image 2 (301 slices, Last 25% - 75 slices)					Image 3 (117 slices, Last 25% - 29 slices)				
		FS	AS	PS	RS	JS	FS	AS	PS	RS	JS
1	Fixed	0.82	1	0.86	0.79	0.79	0.74	1	0.76	0.73	0.7
2	Sauvola	0.01	0.86	0.01	0.01	0.01	0.01	0.87	0.01	0.02	0.01
3	Ni Black	0.21	0.9	0.67	0.13	0.13	0.1	0.94	0.32	0.07	0.06
4	Isodata	0.82	1	0.86	0.8	0.79	0	0.95	0	0	0
5	Local	0.41	0.95	0.52	0.37	0.35	0.34	0.95	0.33	0.39	0.27
6	Local-71	0.68	0.98	0.74	0.65	0.63	0.44	0.96	0.42	0.56	0.38

The next best performing thresholding method is Local-71 method. The local-71 method uses a block size of 71 in comparision with local method which uses a block size of 35. Isodata method performs well for image 0 and 2 and not so well for others.

Out of all the approaches Fixed thresholding approach outperforms the other automatic thresholding approaches consistently by producing comparable results in all quadrants in all types of images. This implies that irrespective of the differences in hounsfield unit values and varying imaging apparatus, the intensity value of the lung region remains constant and using this constant value is more effective than applying histogram based automatic thresholding approaches to find the threshold to segment the lung.

While it is true that fixed thresholding approach outperforms all other methods, it is also worthwhile to check if there are any other thresholds other than -400 when fixed thresholding approach is considered. In image 0 volume the range of voxel intensities vary from -933 to 2667. Beginning at one extreme the threshold was varied at a span of 50 Hounsfield unit such as -933, -883, -833 and so on until it is less than 2667. For each of these thresholds the sensitivity, specificity, precision and recall were calculated to plot the ROC curve (false positive rate vs true positive rate) and the recall vs precision curve as shown in figure 3.

The ROC curve shows a maximum value of accuracy at -133 but the accuracy was becoming more than 95% between -483 and -133 and decreases afterward

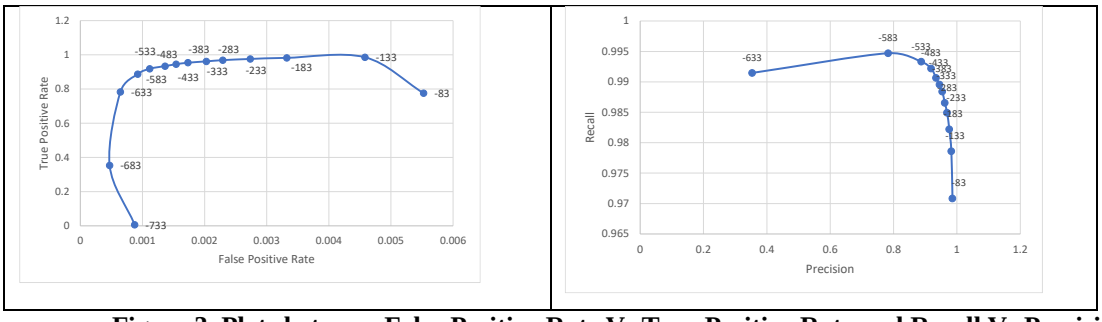

Figure 3. Plots between False Positive Rate Vs True Positive Rate and Recall Vs Precision

Figure 3 also shows the recall-precision curve. Generally, it is desirable that an algorithm should have high precision as well as high recall. The tradeoff between these two with various thresholds is for a fixed thresholding is as shown in figure. When two algorithms are compared, a better algorithm has greater area under curve.

V. Conclusion

This work presented and evaluated the application of different thresholding techniques in a common lung segmentation pipeline to validate the application of fixed thresholding for lung segmentation. This work also compared a mix of various thresholding approaches in a novel quadrant format by dividing the scan volume into four 25% quadrants and producing the results on five evaluation metrics and

comparing all methods across each of these quadrants. It can also be inferred that, the main reason for the failure of automatic thresholding approaches to properly segment lung parenchyma is that at 2D slice level, they are affected by the variations in the intensity distributions and this also explains why fixed thresholding works better than histogram based thresholding approaches. This work can be further extended by applying the thresholding approaches on 2D images available in the dataset.

VI. Acknowledgements

Authors would like to thank Kiran Division, Department of Science and Technology for funding this work and ABV-IIITM Gwalior for facilitating the same. The file number is SR/WOS-A/ET-153/2017.

VII. References

[1]. http://cancerindia.org.in/cancer-statistics/

[2]. El-Baz A, Beache GM, Gimel'farb G, Suzuki K, Okada K, Elnakib A et al.Computer-aided diagnosis systems for lung cancer: challenges and methodologies. International journal of biomedical imaging 2013.

[3]. Dhara AK, Mukhopadhyay S, Khandelwal N. Computer-aided detection and analysis of pulmonary nodule from CT images: A survey. IETE Technical Review 2012; 29(4):265-275.

[4]. Shariaty F, Mousavi M. Application of CAD systems for the automatic detection of lung nodules. Informatics in Medicine Unlocked 2019; 15:100173.

[5]. Norouzi A, Rahim MSM, Altameem A, Saba T, Rad AE, Rehman A et al. Medical image segmentation methods, algorithms, and applications. IETE Technical Review 2014; 31(3):199-213.

[6]. Lu L, Tan Y, Schwartz LH, Zhao B. Hybrid detection of lung nodules on CT scan images. Medical physics 2015; 42(9) :5042-5054.

[7]. Firmino M, Angelo G, Morais H, Dantas MR,Valentim R. Computer-aided detection (CADe) and diagnosis (CADx) system for lung cancer with likelihood of malignancy. Biomedical engineering online 2016; 15(1): 1-17.

[8]. Saien S, Pilevar AH,Moghaddam HA. Refinement of lung nodule candidates based on local geometric shape analysis and Laplacian of Gaussian kernels. Computers in biology and medicine 2014; 54:188-198.

[9]. Abbas Q.Segmentation of differential structures on computed tomography images for diagnosis lung-related diseases. Biomedical Signal Processing and Control 2017; 33: 325-334.

[10]. Taşcı E, Uğur A. Shape and texture based novel features for automated juxtapleural nodule detection in lung CTs. Journal of medical systems 2015; 39(5):46.

[11]. Li B, Chen K, Peng G, Guo Y, Tian L, Ou S et al.Segmentation of ground glass opacity pulmonary nodules using an integrated active contour model with wavelet energy-based adaptive local energy and posterior probability-based speed function. Materials Express 2016; 6(4): 317-327.

[12]. Shaukat F, Raja G, Gooya A, Frangi AF. Fully automatic detection of lung nodules in CT images using a hybrid feature set. Medical physics 2017; 44(7):3615-3629.

[13]. Zhang W, Wang X, Li X, Chen J. 3D skeletonization feature based computer-aided detection system for pulmonary nodules in CT datasets. Computers in biology and medicine 2018; 92:64-72.

[14]. Senthilkumaran N, Vaithegi S. Image segmentation by using thresholding techniques for medical images. Computer Science & Engineering: An International Journal 2016; 6(1):1-13.

[15]. Sahoo PK, Soltani SAKC, Wong AK. A survey of thresholding techniques. Computer vision, graphics, and image processing 1988; 41(2):233-260.

[16]. Mansoor A, Bagci U, Foster B, Xu Z, Papadakis GZ, Folio LR et al. Segmentation and image analysis of abnormal lungs at CT: current approaches, challenges, and future trends. RadioGraphics 2015; 35(4):1056-1076.

[17]. "2D and 3D lung segmentation | Kaggle", https://www.kaggle.com/ azaemon/2d-3d-lung-segmentation, last accessed 12-06-2020

[18]. https://www.kaggle.com/kmader/finding-lungs-in-ct-data

[19]. Niblack W. An Introduction to Digital Image Processing. PrenticeHall, Englewood Cliffs, NJ;1986 .p. 115–116.

[20]. Sauvola J, Pietikainen M. Adaptive document image binarization, Pattern Recognition 2001;33(2):225-236.

[21]. Velasco FR, Thresholding using the ISODATA clustering algorithm. Maryland Univ College Park Computer Science Center 1979.

ISSN- 2394-5125 VOL 7, ISSUE 15, 2020

[22]. Teng CH, Hsu WH, Busey TA, Schneider B L, Moses K , Zheng WS et al. Local Adaptive Thresholding. Encyclopedia of Biometrics 2009: 939–939. doi:10.1007/978-0-387-73003-5_506.